GEOACTA **37**(2): 178-196 (2013) ISSN 1852-7744

WAVELET ANALYSIS OF THE IONOSPHERIC RESPONSE AT MID-LATITUDES DURING THE APRIL 2000 STORM USING MAGNETOGRAMS AND VTEC FROM GPS

L. I. Fernández[1,3], A. M. Meza[1,3], M. A. Van Zele[2,3]

1. Facultad de Ciencias Astronómicas y Geofísicas. UNLP, Buenos Aires. Argentina.
2. Facultad de Ciencias Exactas y Naturales. UBA, CABA., Argentina.
3. Consejo Nacional de Investigaciones Científicas y Técnicas (CONICET). Argentina.
Email: lauraf@fcaglp.unlp.edu.ar; ameza@fcaglp.unlp.edu.ar; avanzele@gl.fcen.uba.ar

ABSTRACT

In this work we pursue the idea of computing a parameter that allows us to estimate the local ionospheric response to a geospheric event that triggers an ionospheric storm. For that, wavelet technique has been chosen because of its ability to analyze non-stationary signals. The advantage of the time-frequency analysis method called Wavelet Transform resides in providing information not only about the frequencies of the event but also about its location in the time series. Specifically, we compute the Scale Average Wavelet Power (SAWP) of two parameters that describe the local geomagnetic field variation at the Earth surface caused by a geospheric storm and ionospheric response to the storm event. In particular, we propose the time delay between the maximum values of SAWP applied to the *vTEC* (vertical Total Electron Content) and the horizontal component of the geomagnetic field (*H*) variations as parameters to characterize the local behavior of the ionospheric storm.

We applied the parameter to the geomagnetic and ionospheric disturbances caused by a coronal mass ejection (CME) that took place on April 4, 2000. We used *vTEC* values computed from GPS observations and *H* at the surface of the Earth, measured in stations near to each GPS station chosen. The *vTEC* values used came from the GPS permanent stations belonging to the global IGS (International GNSS Service) network. We chose stations located at magnetic mid-latitudes. Moreover, three-longitude bands representing the ionospheric behavior at different local times (LT) were studied.

Because the April 2000 storm has been extensively studied for many authors, the results are compared with those in the literature and we found a very good agreement as expected.
Keywords: Mid-latitude ionosphere, Geospheric Storms, Wavelet Transform, Total electron content, GPS.

RESUMEN

En este trabajo perseguimos la idea de estimar un parámetro que nos permita calcular la respuesta ionosférica local a un evento geosférico desencadenante de una tormenta ionosférica. Para ello, se eligió la aplicación de la técnica ondeleta debido a su capacidad para analizar señales no estacionarias. La ventaja del método de análisis en tiempo y frecuencia llamada Transformada Ondeleta reside en el hecho de que provee información, no sólo acerca de las frecuencias del evento, sino también sobre su ubicación en la serie de tiempo. En concreto, se calcula el promedio por escalas de la potencia de la transformada ondeleta (SWAP, de su sigla en inglés Scale Average Wavelet Power) para dos parámetros que describen la respuesta local de la magnetosfera y la ionosfera a una tormenta. En particular, se propone el retraso de tiempo entre los valores máximos de SAWP aplicadas al *vTEC* (Contenido Electrónico Total en dirección Vertical) y la componente horizontal del campo geomagnético (*H*), como parámetros cuyas variaciones caracterizan el comportamiento local de la tormenta ionosférica.

El parámetro propuesto se aplicó a las perturbaciones geomagnética e ionosférica causadas por una eyección de masa coronal (CME, Coronal Mass Ejection), que tuvo lugar el 4 de abril de 2000. Se utilizaron valores *vTEC* calculados a partir de las observaciones GPS y *H* en la superficie de la Tierra, medida en las estaciones cercanas a cada estación de GPS elegida. Los valores de *vTEC* utilizados provinieron de las estaciones GPS permanentes que pertenecen a la red del servicio internacional IGS (International GNSS Service). Entre todas, elegimos

estaciones situadas en latitudes magnéticas medias. Por otra parte, estudiamos tres bandas de longitud que representan el comportamiento de la ionosfera a distintas horas locales (LT).

Debido a que la tormenta de abril de 2000 ha sido ampliamente estudiada por muchos autores, los resultados se comparan con los de la literatura y nos encontramos con un muy buen acuerdo entre los datos publicados y nuestros resultados, tal y como se esperaba.
Palabras Clave: Ionosfera a latitudes medias, Tormentas geosféricas, Transformada ondeleta, Contenido electronico total (TEC), GPS.

INTRODUCTION

The geospheric storm is an event of strongly enhanced dissipation of solar wind energy where all regions between the Earth and the Sun are affected. According to Prölss (1995) a geospheric storm refers to a strong dissipation of solar wind energy in the near-Earth environment that lasts for 1 to 3 days. This phenomenon usually links a solar event with upper atmospheric disturbances and involves both magnetospheric and ionospheric storms.

Nowadays, it is accepted that the magnetic reconnection is an important process of solar wind energy transfer to the magnetosphere (Tsurutani et al., 2001). After a Coronal Mass Ejection (CME) event, solar plasma attached to the Interplanetary Magnetic Field (IMF) lines is flowing to the Earth. At the dayside, the southward component of the IMF leads to reconnection with the northward magnetopause magnetic field leading to injection of solar wind energy into de magnetosphere (Tsurutani et al., 2001). Then, the charged particles from interplanetary plasma and part of magnetospheric plasma, following the open field lines can penetrate the atmosphere, drift together across the polar region (Prölss, 2004). A magnetospheric storm is the perturbation that follows in the magnetosphere when solar particles with high velocity or/and density impinge on the magnetopause. The entrance of solar particles into the magnetosphere produces the enhancement and acceleration of plasmaspheric particles which increase the ring current. A geomagnetic storm is the variation of geomagnetic field during a magnetospheric storm.

An ionospheric storm generally refers to the disturbances in the ionosphere during a geomagnetic storm. In particular, this term refers to perturbations in the *F* region (Prölss 2004; Mendillo, 2006; Lastovicka, 2002) in terms of the ionospheric peak electron density (N_mF_2) and the height at which the peak occurs ($h_m\ F_2$) and its pattern depends on latitude, season and local time (LT). The *vTEC* (vertical Total Electron Content) is the ionospheric electron content in a unit vertical column. Thus, *vTEC* is a parameter widely used to describe the integrated behavior of the Ionosphere. Specifically, *vTEC* values determined from GPS (Global Positioning System) measurements used in our presentation were obtained from double-frequency GPS receivers that belong to IGS network.

Several papers (Mendillo, 2006 and references therein) characterize an ionospheric storm at mid-latitudes from vTEC departures from average or quiet behavior.

The characteristic features of each storm are as unique as a fingerprint. However, at geomagnetic mid-latitudes some stages related to the LT, common to the majority of them, can be distinguished. Thus, a chosen storm could have only a positive phase, a positive and a negative phase or it could be just a negative storm with no positive phase. Nominally, the ionosphere exhibits strong spatial gradients across the sunrise terminator linked to the photoionization. According to Mendillo (2006), the storm intensifies these known processes up to extend not fully known.

Among the physical causes of the negative and positive phases of an ionospheric storm we can mention the following: electrodynamical and termospheric mechanisms are thought to lead a positive phase, whereas enhanced ionospheric chemical loss driven by changes in the thermosphere is responsible of the negative phase.

The negative storm effect is the most crucial and consistent feature of the ionospheric storms at mid-latitudes (Tsagouri and Belehaki, 2006). About the negative phase, there is an agreement in assigning its magnetospheric origin. Effectively, the high latitudes heating that provokes neutral circulation from high to low latitudes has the result of enriching the molecular nitrogen concentration (N_2) at mid-latitudes, and making poor the atomic oxygen concentration *(O)* at low latitudes. These two neutral gases density changes cause the decrease of the ionization density rate in the F region. Actually, at one hand the low *O* density produce a decrease in the oxygen ions production rate. On the other hand, the increase of the N_2 density causes an increase in the ions loss rate. These two causes combined decrease the ionization density of the F region (Prölss, 1995; Mendillo, 2006).

The origin of the positive phase is still not completely clear. Two mechanisms have been proposed as responsible of the positive ionospheric storms at mid-latitudes: winds in the neutral atmosphere and electric field (Swisdak et al, 2006). The former reason is clearly explained by Prölss. According to Prölss (1993, 2004), the positive phase is a predominantly daytime phenomenon caused by TADs (Travelling Atmospheric Disturbances). These are disturbances caused by atmospheric gravity waves propagating at high velocities (500-1000 m/sec) from polar to equatorial regions. Such disturbance propagates with storm induced winds and pushes the F region

upwards following the geomagnetic field lines at geomagnetic mid-latitudes, causing thus a density disturbance (Prölss, 2004; Fuller-Rowell et al, 1994; Jakowski et al, 1990, Lu et al., 2001; Swisdak et al., 2006). The hot point of this theory is the typical duration of a positive phase attributed by a TAD origin. Following (Prölss, 2004), a TAD passing from ~70º in latitude to the equator takes about 3-4 hours. This mechanism also considers the encounter of the original TAD with another one in opposite direction causing compression, heating and more density changes.

On the other hand, Foster (1993) asseverated that during storm conditions electric field convects high density plasma from lower to higher mid-latitudes producing thus an increase in ionization density. Later, Werner et al. (1999) affirmed that storm heating of the thermosphere results not enough to explain this effect. Huang et al. (2005) agreed with the quick propagation of the electric field to low latitudes. They had taken measurements of incoherent scatter radar and TEC values from the global GPS network and observed a minimal lag between the geomagnetic storm onset and the ionospheric response in the analyzed data. Moreover, Meza et al. (2005) using *vTEC* from GPS, recorded variations of the geomagnetic field and the geomagnetic indexes Dst and AL, also found out a simultaneous response of the ionosphere and the geomagnetic field during geospheric storms.

Foster and Rich (1998) reported direct observations of the uplift of the ionosphere at mid-latitudes caused by a Prompt Penetration of the Electric Field (PPEF) eastwards. Swisdak et al. (2006) asseverated that both processes could probably live together and be complimentary because the neutral winds can maintain a dynamo electric field.

Balan et al. (2010) presented a physical mechanism to explain the positive storms involving both electric field and neutral winds. The authors set up that a daily eastward PPEF along with an equatorward neutral wind are required to produce positive storms at low and mid geomagnetic latitudes. Effectively, the **E** x **B** drift needs the effects of neutral winds to raise the ionosphere to high altitudes of reduced chemical loss and near the ionospheric peak ($h_m F_2$). Besides the wind reduces the downward diffusion of plasma along the geomagnetic field lines (Balan et al., 2010). The authors concluded that the positive ionospheric storms are preferable expected at latitudes up to ± 30º where the daytime east PPEF can shifts the equatorial anomaly crest; and at longitude sectors where the onset of the geomagnetic storm occurred at morning-noon. In this scenario, the plasma accumulation caused by equatorial neutral winds largely exceeds the plasma loss due to recombinations as chemical effects of the wind.

The April 2000 event refers to the geospheric storm triggered by a coronal mass ejection (CME) that took place on 4 April 2000 near to the western limb of the Sun (Huttunen et al., 2002). Since this storm came after a relatively quiet geomagnetic activity and it is not superposed by another clear perturbation, this equinoctial event has been widely studied during the past ten years by several authors. Effectively, the selected storm was geomagnetically characterized by an SSC, preceded by a slightly disturbed day and without the arrival of a new solar rapid flow during its phase of expansion or of recovery, that is, a new storm is not superimposed.

Perhaps the most extensive study of the April 2000 event was performed by Huttunen et al. (2002). The authors analyzed the geospheric storm completely starting from the CME close to the western limb of the Sun on 4 April 2000, the magnetic activity two days after and finishing with the analysis of the induction phenomena driven by ionospheric currents linked to the geomagnetic storm in the Finnish natural gas pipeline (Huttunen et al., 2002).

Afraimovich et al. (2002) also studied the atmospheric response to the major geomagnetic storm of 6-8, April 2000. For their work, they used *vTEC* from GPS stations in Russia and central Asia as well as optical observations and established a correlation between them at periods of about 4-42 hours. They affirmed that the origin of this correlation is the heating of the F-region due to energetic particle precipitation in the auroral ionosphere and the large-scale traveling ionospheric disturbances associated. The 6-7 April 2000 magnetic storm produced a magnificent aurora that was seen in Central Europe (Huttunen et al., 2002). Afraimovich et al. (2002) compared the enhancement in optical 630 mm. emission in the frequency range 1-2 mHz. with dynamic spectra of TEC variations.

Liu et al. (2004) analyzed the low latitude ionospheric responses of April 2000 storm by using three digisondes near the longitude 120º E. They studied the PPEF and the wave-like disturbances induced by the storm.

Lee et al. (2004) used three ionosondes and satellite data to analyze the TADs caused by the before mentioned storm. Moreover the authors compare the observations with model simulations.

Kumar et al. (2006) studied interplanetary parameters and F_2-region responses using ionosonda data from a low latitude station for more than one hundred geospheric storms during 1997-2000. Although the conclusions are statistical, the authors had devoted a careful analysis to the April 2000 event.

More recently, Huang (2008) and Abreu et al. (2010) studied the same storm but focused on the equatorial and low latitude sectors. Abreu et al. (2010) used GPS TEC data from four stations in Brazil and ion density measurements from two satellite missions. The authors detected storm-induced big plasma bubbles and analyze the positive/negative phases of the ionospheric storm at magnetic latitudes up to 20º.

The idea of cross-correlation analysis between some geomagnetic index and TEC variations as a way to analyze the ionospheric answer to geomagnetic activity perturbations had been recently developed. In fact Liu et al. (2010) studied the cross-correlation between geomagnetic disturbances and TEC responses for ionospheric storms. In particular the authors studied the relationship between the intensity of the geomagnetic perturbation and the time

duration and the time delay of the positive and/or negative phase of the ionospheric storm. In the same way, Andonov et al. (2011) applied cross-correlation analysis between VTEC and K_p index as an indicator of geomagnetic activity for the North America region. Both authors reported that the relationship between geomagnetic perturbations and the appearance and the time duration of the positive and/or negative phase of the ionospheric storm are conditioned by solar activity, season, latitude and LT of the station.

In this work, we choose the extensively studied event of April 2000 to test a wavelets application. We propose a parameter to quantify some features characterizing the geospheric storm. For that, we compute the time delay between the maximum values of average wavelet power spectrum applied to GPS *vTEC* and *H* variations. In particular we use GPS measurements to explore the ionospheric response to the 4-8 April 2000 geospheric storm at geomagnetic mid-latitudes and at different LTs.

Section 2 gives a brief description of the parameters that characterized the geomagnetic intense storm, follows data processing procedures and mathematical methods involved. Section 3 provides the analysis of the results and Section 4 presents a discussion and summary of results.

METHODOLOGY

The April 2000 event was considered as the largest magnetic storm of the year 2000 (Huttunen et al., 2002). The geospheric storm started with a CME on 4 April, but we focused the analysis on the geomagnetic event that took place two days after. The magnetic storm started on 6 April 2000 with a sudden storm commencement. The sudden variation is reported at 16:39 UTC (Bulletin Mensuel n° 00-04-Avril 2000 du Service International des Indices Geomagnetiques, France; hence after named as Bull0400). The selected event is an isolated storm (Bull0400) that was preceded by slightly disturbed days according to the *Km* indexes (Menvielle and Berthelier, 1991, Bull0400). The *Km* index is an “improved *Kp*” mid-latitude geomagnetic activity index computed at 3-hour UTC intervals, available from 1959 at the Bureau del Publications du Service International des Indices Geomagnetiques (http://isgi.cetp.ipsl.fr). The improvements over *Kp* come from the greater number and better distribution of the contributing observatories. So, *Km* represents a better mean value of the disturbances levels in the two horizontal field components, although their differences with the *Kp* are not significant.

Figure 1 shows from 4 April 2000, 00:00 UT till 8 April 2000, 23:59 UT: the vertical component of the interplanetary magnetic field (Bz(IMF)); the solar wind pressure at 1 AU (http://cdaweb.gsfc.nasa.gov/) and the SYM-H index (Iyemori, 2000). We used this index instead of the well-known disturbance storm time (Dst) index since its one-minute resolution transforms it into a tool better adapted for the treatment of sporadic episodes of short duration such as a geospheric storm. Obviously SYM-H index resembles the Dst index behavior although it is obtained from a different set of stations and a different coordinate system.

It can be seen on Fig.1, the SSC arrives at the time indicated as 64:46 hours on the graphic (it corresponds to 6 April, 16:46 UT) and the pressure remains high till 9:00 UT of the next day. Before the SSC the solar pressure was quiet but the Bz(IMF) (Top) changes repeatedly its sign, producing the perturbation shown by the *Km* index (Bull0400). At 16:45 UT Bz(IMF) turns negative and it do strongly at 17:45 UT by some 7 hours, opening the magnetosphere and allowing the entry of solar particles. Subsequently, short intervals with Bz(IMF) < 0 are recorded on 7 April between 5:17 and 6:50 UT. From Fig 1 (bottom), the SYM-H index showed a sharp increase on 6 April, 16:39 UT (SSC) (http://wdc.kugi.kyoto-u.ac.jp/aeasy/index.html) followed by a decrease displaying the growth of the equatorial ring current at 16:46 UT, that reach 3 close minima on 6 April: -290 nT at 22:57 UT, -306 nT at 23:12 UT and -320 nT on 7 April at 00:09 UT.

Essentially, when Bz(IMF)<0, the magnetosphere is open, that is, it admits the incoming of solar wind particles. When the solar wind pressure increases, also increase the number of incoming particles. Thus, the ring current intensifies producing an intense decrease of *H* and *X* components. The SYM-H index, representing the symmetric ring current, adopts negative values. When, Bz(IMF)>0 the magnetosphere is closed and the energetic particles only income at the poles. When this is the case, the ring current decays and the SYM-H index slowly recover the values previous to the storm. Huttunen et al (2002) analyzed the same phenomenon and they found several intense episodes normally linked to triggers of intense sub storms, which appeared during the whole storm and they owe only to variations in the solar wind.

Tsagouri and Belehaki (2006) showed that a ionospheric storm can be locally divided by the amplitude of the ionospheric response as a function of LT of the observation point in 4 sectors: the pre-noon sector (6:00 to 12:00 LT); the afternoon sector (12:00 to 18:00 LT); the evening/midnight sector (18:00 to 21:00 LT) and the morning sector (21:00 to 3:00 LT). They found out that according to the Earth rotation the ionospheric response increase in clockwise direction from midnight.

With the aim of studying the different behavior of the ionosphere at different LT, we considered three longitude-bands. Thus, the disturbance was regarded by A1 area at noon sector, A2 area at afternoon-evening sector and A3

area during the morning sector. Besides, the geomagnetic observatories and GPS stations are located at geomagnetic mid-latitudes in both hemispheres.

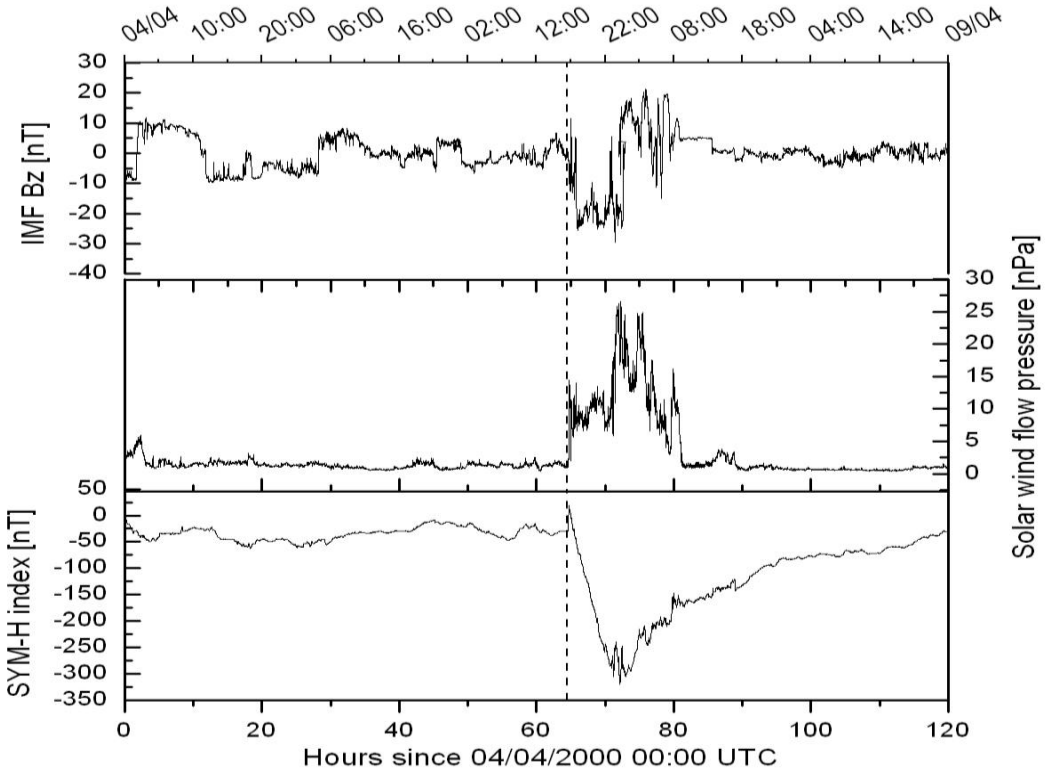

Figure 1. From top to bottom: the vertical component of the Interplanetary Magnetic Field (IMF Bz); the solar wind pressure at 1 AU; and the SYM-H index for the period 4-8 April 2000 as a function of time [hours] since 4 April 2000, 0:00 UTC. The instant of the SSC is also marked in thick dotted line.

Figura 1. Desde arriba hacia abajo**:** Componente vertical del campo magnético interplanetario (IMF Bz); Presión del viento solar a 1 unidad astronómica (1 AU); y el índice SYM-H en función del tiempo [horas] para el periodo del 4 al 8 de abril del 2000. La grafica comienza el 4 de abril de 2000 a las 0:00 UTC. El instante del SSC se marca como una línea punteada gruesa.

Figure 2 shows the locations of GPS receivers and geomagnetic observatories located at mid latitudes in the northern and southern hemispheres. The respective geodetic and geomagnetic coordinates of the selected observatories are given in Tables 1 and 2.

To analyze the effect of the geospheric storm on the geomagnetic field and the ionosphere at magnetic mid-latitudes locations, we used the variation of the horizontal component of the geomagnetic field (d*H*) and the variations of *vTEC* (d*VTEC*) as parameters. These parameters are generated using the nearest quiet day as a reference. In order to compare them geomagnetic observatories close to a selected GPS receiver are chosen.

Data Analysis

To assess geomagnetic and ionospheric disturbances the horizontal component of the geomagnetic field at the Earth surface and vertical Total Electron Content (*vTEC*) from Global Positioning System (GPS) measurements at mid-latitudes locations were used.

In our analysis the geomagnetic and ionospheric variations are defined as the difference between magnitudes recorded during the day chosen and the corresponding magnitude for a geomagnetically quiet day. The last is repeated for all days used in our analysis. The differences are taken at the same UT and they allow us a comparative study between quiet and disturbed days. The quiet geomagnetic day has to be close to the period 4-8th April 2000; so 14th April 2000 was chosen as quiet day of reference for ionospheric and geomagnetic data ($\sum Km = 5+$ and the eight *Km* are lower than 2).

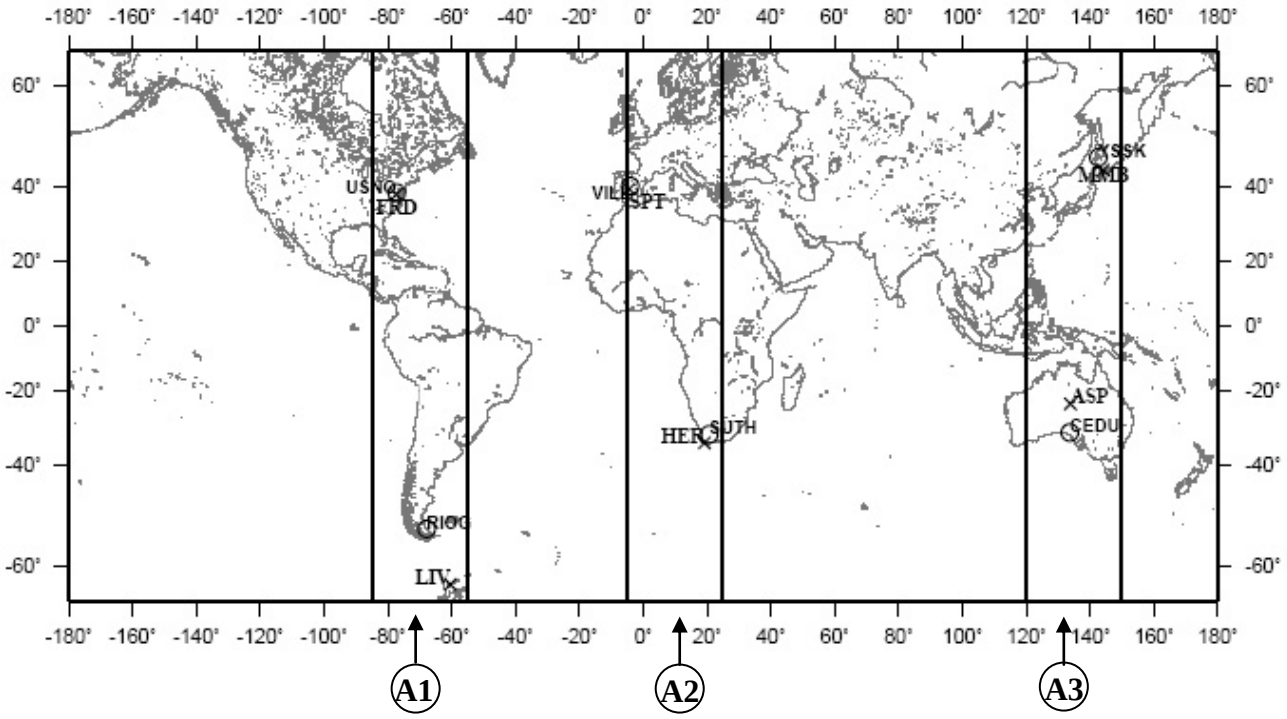

Figure 2. Map of the location of geomagnetic (crosses) and GPS stations (open circles).
Figura 2. Mapa de la ubicación de las estaciones geomagnéticas (cruces) y GPS (círculos abiertos).

Storm: 16:39UT		Local Time	GPS station			
			Name	Geomagnetic latitude	Geographic latitude	Geographic longitude
A1	**North**	11:39	USNO	48.97º	38.92º	77.07º W
	South	13:39	RIOG	-43.82º	-53.78º	67.75º W
A2	**North**	17:39	VILL	43.46º	40.44º	3.95º W
	South	18:39	SUTH	-32.35º	-32.38º	20.81º W
A3	**North**	3:39	YSSK	38.59º	47.03º	142.72º E
	South	3:09	CEDU	-40.72º	-31.87º	133.82º E

Table 1. Location of the GPS stations divided in three areas (A1, A2 and A3).
Tabla 1: Ubicación de las estaciones GPS divididas en tres áreas (A1, A2 and A3).

Storm: 16:39UT		Local Time	Geomagnetic observatory			
			Name	Geomagnetic latitude	Geographic latitude	Geographic longitude
A1	**North**	11:39	FRD	48.10º	38.20º	77.37º W
	South	13:39	LIV	-52.84º	-62.66º	60.39º W
A2	**North**	17:39	SPT	42.64º	31.55º	4.35º W
	South	18:39	HER	-34.08º	-34.42º	19.23º E
A3	**North**	1:39	MMB	35.63º	43.10º	144.19º E
	South	3:09	ASP	-32.64º	-23.76º	133.88º E

Table 2. Location of geomagnetic stations, divided in three areas (A1, A2 and A3).
Tabla 2: Ubicación de las estaciones geomagnéticas divididas en tres áreas (A1, A2 and A3).

The *vTEC* was computed using the methodology describe by Meza et al (2005) and Gomez et al (2007) using the GPS RINEX data.

Finally the *vTEC* for the selected station were obtained for both the disturbed and quiet days. Consequently the *vTEC* variations parameter (d*VTEC*) was defined as:

$$dVTEC(t) = vTEC(t) - vTECqq(t) \quad (1)$$

where *vTECqq* is the *vTEC* during a quiet day, and *t* is Coordinated Universal Time (UTC).

In relation with the geomagnetic field, the variations of *H (dH)* are obtained using the measured (*X, Y*) components. Thus,

$$dX(t) = X(t) - X_{qq}(t)$$

$$dY(t) = Y(t) - Y_{qq}(t) \quad (2)$$

$$dH(t) = \sqrt{X(t) - X_{qq}(t)^2 + Y(t) - Y_{qq}(t)^2}$$

where (X_{qq}, Y_{qq}) are the (*X, Y*) components during a quiet day, and *t* refers to Coordinated Universal Time (UTC).

Wavelet analysis

Both Fourier and Wavelet Analysis can measure the time-frequency variations of spectral components. Nevertheless only the wavelet algorithms can manage data at different scales or resolutions. The wavelet analysis is suitable to analyze turbulent or short-period phenomena in signals (Mendes et al., 2005; Boudouridis and Zesta, 2007). The principal advantage of the time-frequency analysis method called Wavelet Transform (hereafter WT) over the conventional Fourier Analysis resides in providing information not only about the frequency of the event but also about its location in the time series. The WT refers to an integral transform using wavelets as integration kernels for analysis to extract information about the process (Kumar and Foufoula-Georgiou, 1997). An extensive overview of the WT properties and their common geophysical applications can be found in (Daubechies, 1992; Kumar and Foufoula-Georgiou, 1994, 1997, Holschneider, 2000).

Defining the Morlet mother wavelet as,

$$\psi(t) = \frac{e^{i\omega_0 t}}{\sqrt[4]{\pi}\, e^{t^2/2}}, \quad (3)$$

where *t* is time and ω_0 is set equal to 6 to fulfill the admissibility condition. A family of wavelets is generated from Eq. (3) by scaling and translating the mother wavelet. Thus, a family of Morlet wavelets is:

$$\psi_{a,b}(t) = \frac{1}{\sqrt{a}}\psi\left(\frac{t-b}{a}\right), \quad (4)$$

where *b* denotes the shift parameter; *a* the scale and the normalization factor $a^{-1/2}$ guarantees equal energy at different scales (Ge, 2007). The continuous Morlet WT of a discrete equal time space data series *x(t)* is defined as

the convolution of the data series with the family of the Morlet wavelets (Kumar and Foufoula-Georgiou, 1997; Torrence and Compo, 1998)

$$WT(a,b) = \int_{-\infty}^{\infty} x(t)\,\psi^{*}_{a,b}(t)\,dt\,, \tag{5}$$

where (..)* refers to the complex conjugate. In a discrete form, the expression for the wavelet coefficient at time index *n* and scale *a* (Torrence and Compo, 1998; Ge, 2007)

$$W(a) = \sum_{n'=0}^{N-1} x(n')\,\psi^{*}\left[\frac{(n'-n)\delta t}{a}\right], \tag{6}$$

where *N* is the length of the data time series and δt is the sampling period.

The confidence of the WT results is given by the cone of influence, which delimits the region where the errors of the edge effects are important. Any pick out of the cone of influence have to be dismissed. The edge effect is a consequence of the zero-padding of the time series.

In order to analyze fluctuations in power over a band of scales, we used the Scale-Averaged Wavelet Power (SAWP) as defined by Torrence and Compo (1998)

$$\bar{W}_n^2 = \frac{\delta j\,\delta t}{0.776} \sum_{j=j1}^{j2} \frac{\left|W(a_j)\right|^2}{a_j}\,, \tag{7}$$

where δj is a factor related to the width in spectral-space of the wavelet mother function: the smaller δj, the finer wavelet power spectrum resolution (Torrence and Compo, 1998). Notice that Eq. (7) is the weighted sum of the wavelet power spectrum over scales a_1 to a_2. In this work we used the band from 0.5 to 24 hours to characterize the frequency behaviour of the magnetospheric and ionospheric storm. It is because the ionospheric phenomenon (d*vTEC*) is showing not significant power for periods below 0.5 hours and the limit of 24-hour period is enclosed by the cone of influence.

RESULTS

Figures 3, 4 and 5 show the respective data time series of *vTEC* and *H* variations (d*vTEC* and d*H*) and the corresponding wavelet power spectrum along with the Scale-Averaged Wavelet Power over 0.5-24 hours, for the three chose longitude-bands. As expected, we can observe a different behaviour of the ionosphere linked to the local time of the geomagnetic storm onset.

According to Prölss (2004), during a storm additional high pressure areas form in the polar zones that are heated by particles precipitation and electric currents from solar wind energy interacting with the upper atmosphere. Such polar heating zones induce winds with increased molecular species which are superposed onto the normal diurnal wind circulation. The transport of the density perturbations in the neutral atmospheric components due to the storm is also different at different local times. In the night sector, additional high pressure areas induced additional storm winds amplifying thus the equatorward atmospheric circulation. In the day sector, the carrying of the density perturbations is shunned by the poleward directed winds. Following Mendillo, (2006), the same ionospheric storm can show both positive and/or negative phase during the same day and in the same hemisphere at mid-latitudes but separated in longitude, that is, at different local times. As an example, he showed that if the storm starts early in local time, during the time the storm develops the station goes to the afternoon sector. Because the neutral composition changes that increase the electrons loss in the negative phase acts quickly and the photoionization becomes ineffective, hence only the negative phase could be recorded for such station. At noon in both hemispheres, a positive phase appears (Fig. 3a and 3b). It is followed by a negative phase, whereas at dusk-evening (Fig. 4a and 4b) and night (Fig. 5a and 5b) only the negative phase is observed. The reasons are in the chemical loss due to neutral winds which largely exceeds the ionization production related to the solar radiation. On the other hand, the response of the magnetic field is more seemed in the three cases.

Liu et al. (2010) calculated duration and time delay of ionospheric disturbances by applying a classical cross-correlation function between an interpolated *Ap* index time series and TEC variations from IONosphere maps EXchange files (IONEX) data. Thus, the cross-correlation values took positive and negative values.

Different to this, we can quantify the intensity of the local ionospheric response with respect to the geomagnetic perturbations by using the SAWP, which is always positive. Besides, we can also estimate the time delay of the maximum ionospheric response by computing a normalized cross-correlation index of the ionospheric and geomagnetic SAWP time series.

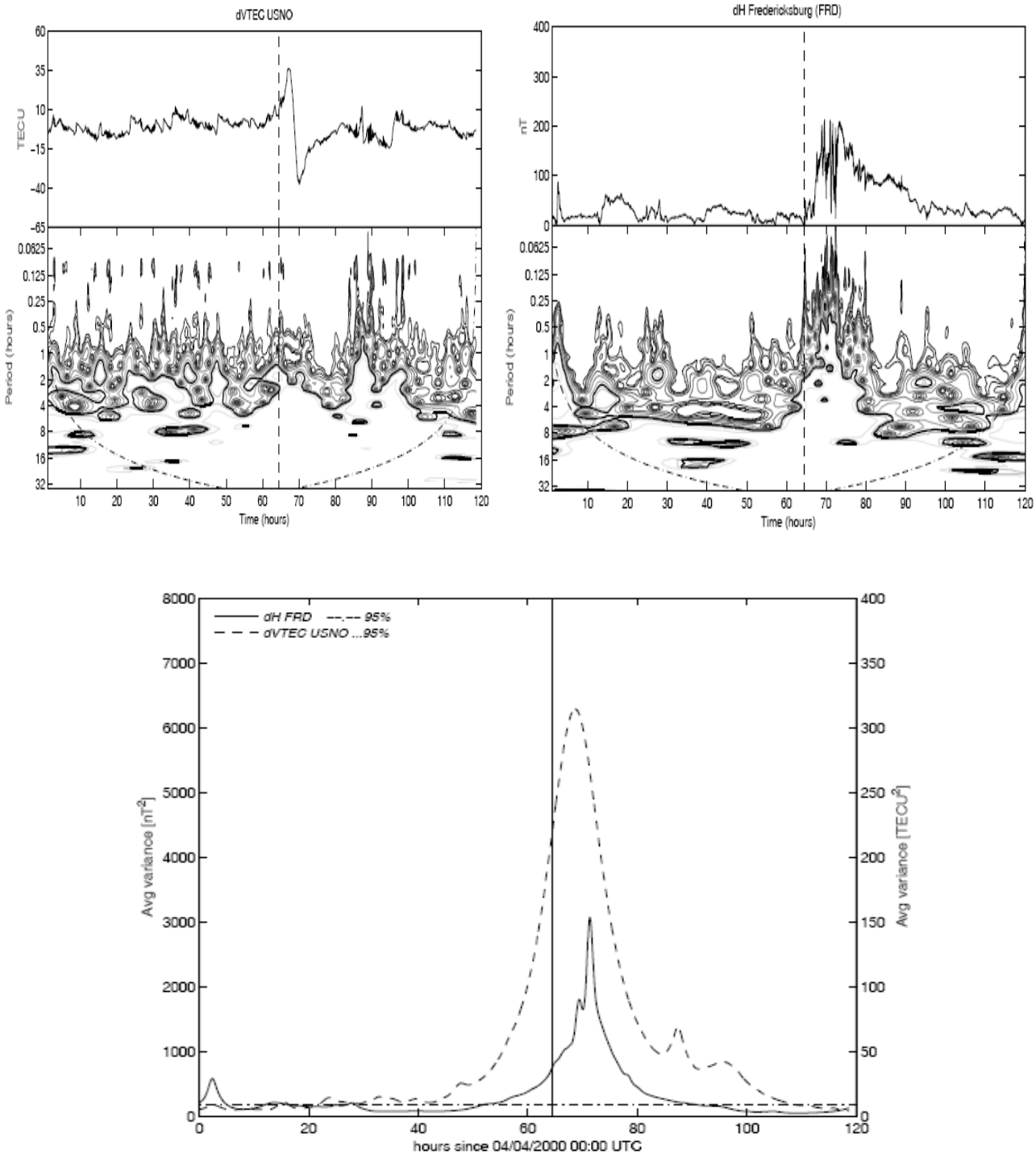

Figure 3a. *VTEC* and *H* variations for the GPS station (left) and the respective geomagnetic observatory (right) corresponding to the northern part of the A1 region. Each plot shows the data time series and the wavelet power spectrum. Below the SAWP over the 0.5-24-hour band for *H* (solid) and *VTEC* (dashed) variations. The thin dashed line is 95% confidence interval for d*H* and the dash pointed line is the 95% level for d*VTEC*. The vertical solid line indicates the time of the storm commencement.

Figura 3a. Variaciones de *VTEC* y *H* en la estación GPS (izquierda) y el respectivo observatorio geomagnético (derecha) correspondientes a la parte norte de la región A1. Cada grafico muestra la serie temporal de datos y espectro de potencia ondeleta correspondiente. Debajo se muestra el SAWP (el promedio por escalas de la potencia ondeleta) para la banda de 0.5 a 24 horas calculada para las variaciones de *H* (línea solida) y *VTEC* (línea de segmentos) respectivamente. La línea punteada fina representa el 95% del intervalo de confianza para d*H* y la línea de puntos y rayas corresponde al nivel de 95% para d*VTEC*. La línea vertical solida indica el instante de comienzo de la tormenta.

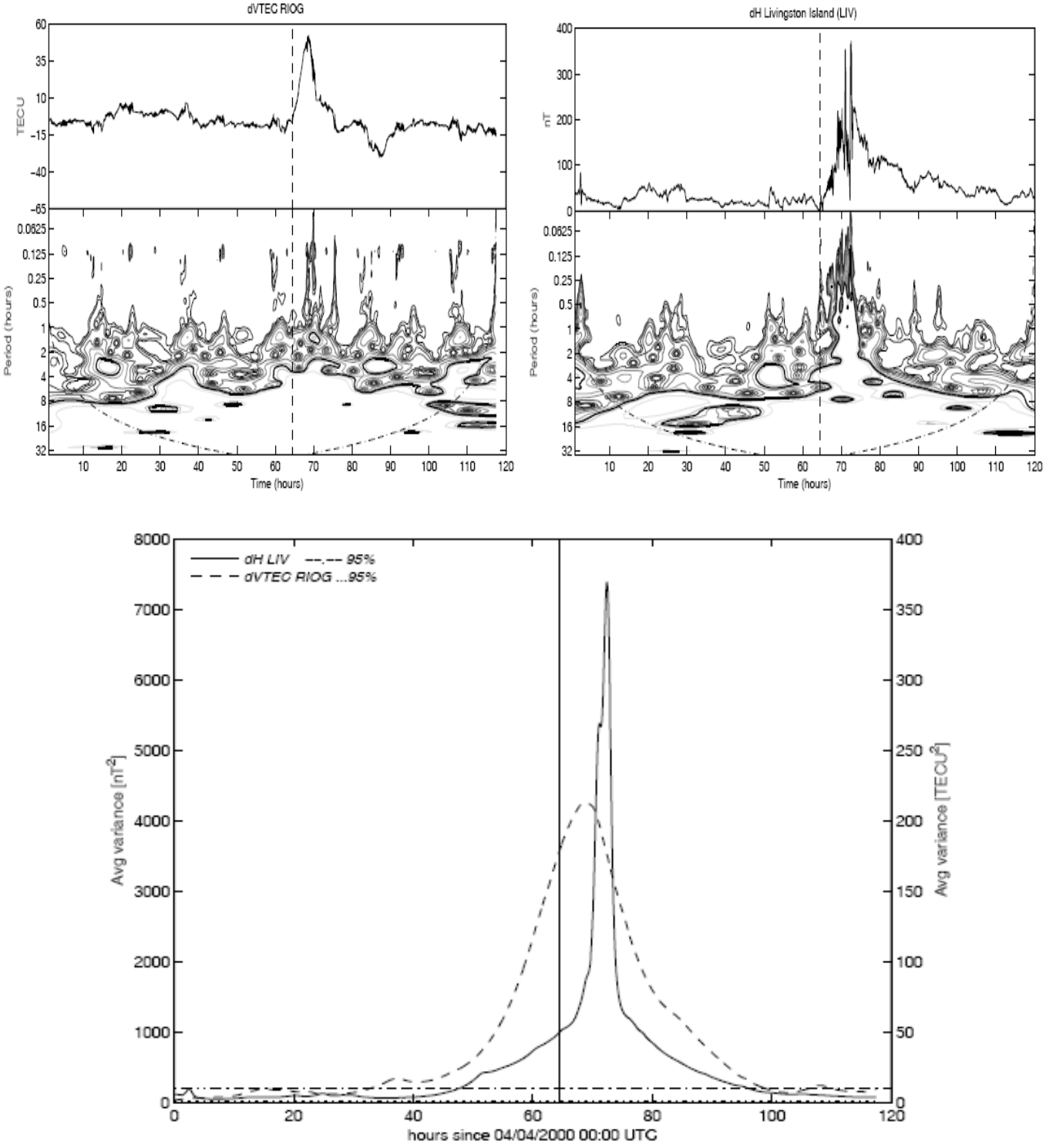

Figure 3b. The same as Fig. 3a for the southern hemisphere
Figura 3b. Lo mismo que la Fig. 3a para el hemisferio austral

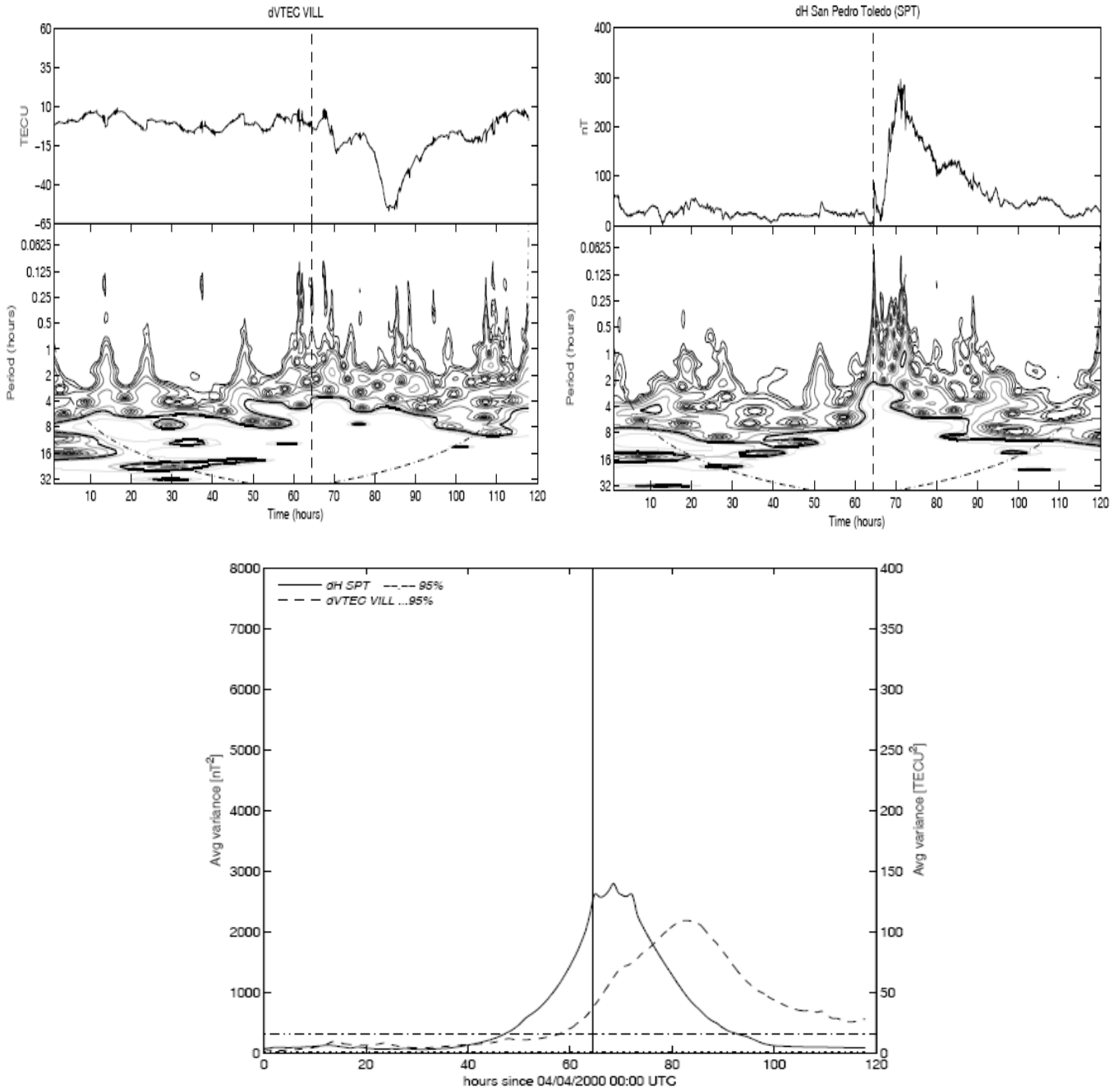

.

Figure 4a. *VTEC* and *H* variations for the GPS station (left) and the respective geomagnetic observatory (right) corresponding to the northern part of the A2 region. Each plot shows the data time series and the wavelet power spectrum. Below the SAWP over the 0.5-24-hour band for *H* (solid) and *VTEC* (dashed) variations. The thin dashed line is 95% confidence interval for d*H* and the dash pointed line is the 95% level for d*VTEC*. The vertical solid line indicates the time of the storm commencement.

Figura 4a. Variaciones de *VTEC* y *H* en la estación GPS (izquierda) y el respectivo observatorio geomagnético (derecha) correspondientes a la parte norte de la región A2. Cada grafico muestra la serie temporal de datos y espectro de potencia ondeleta correspondiente. Debajo se muestra el SAWP (el promedio por escalas de la potencia ondeleta) para la banda de 0.5 a 24 horas calculada para las variaciones de *H* (línea solida) y *VTEC* (línea de segmentos) respectivamente. La línea punteada fina representa el 95% del intervalo de confianza para d*H* y la línea de puntos y rayas corresponde al nivel de 95% para d*VTEC*. La línea vertical solida indica el instante de comienzo de la tormenta.

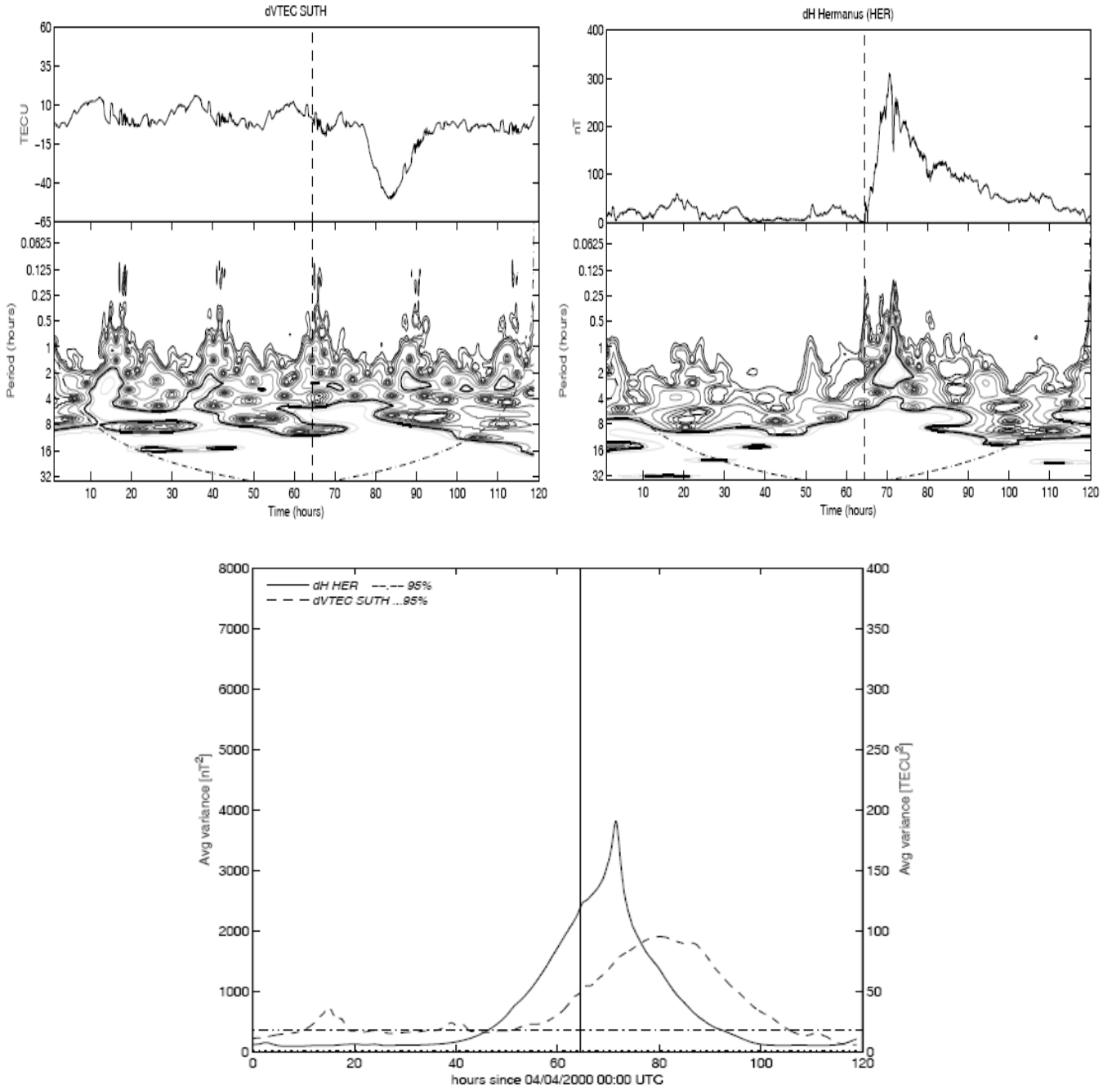

Figure 4b. The same as Fig. 4a for the southern hemisphere.
Figura 4b. Lo mismo que la Fig. 4a para el hemisferio austral.

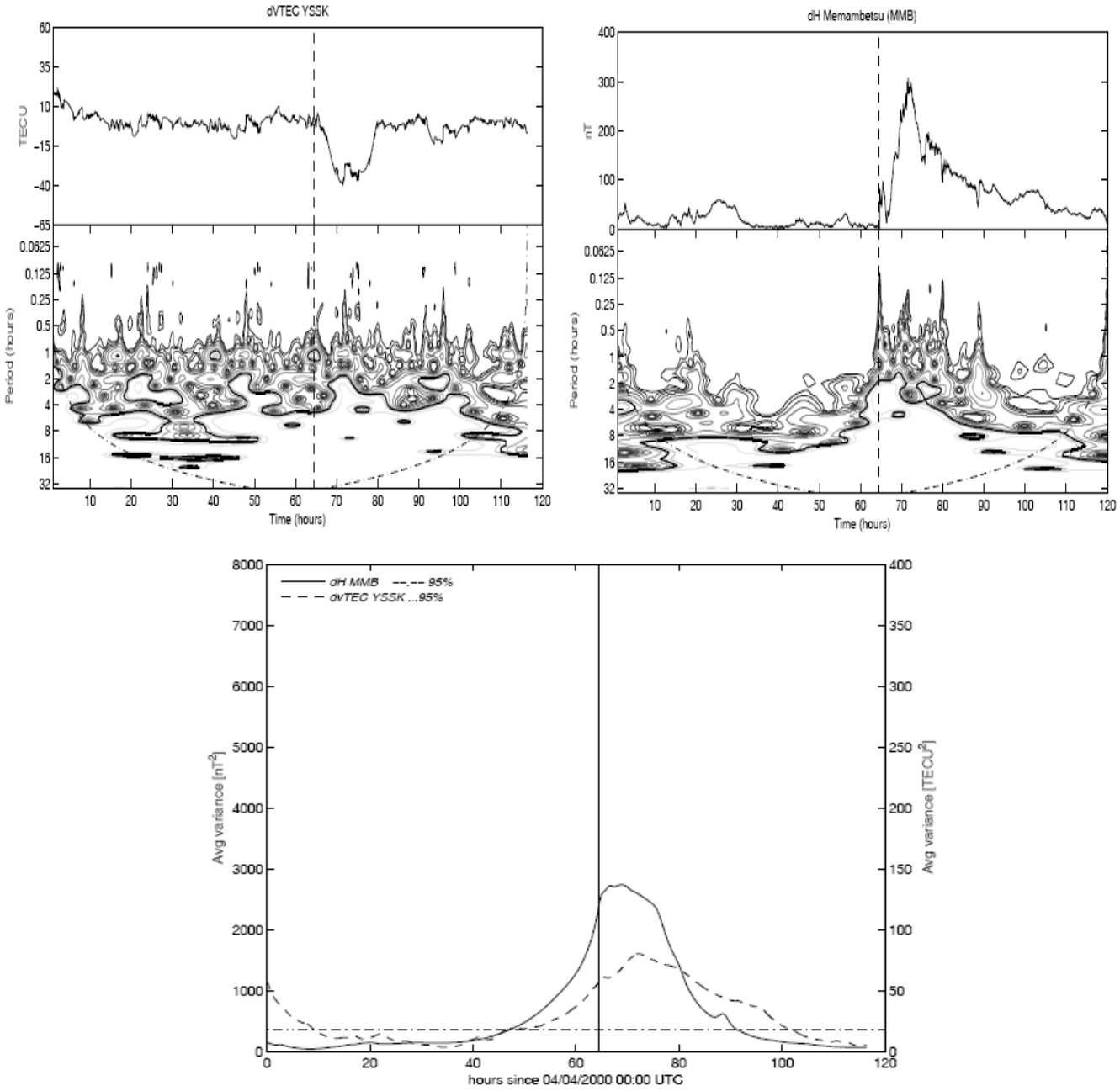

Figure 5a. *VTEC* and *H* variations for the GPS station (left) and the respective geomagnetic observatory (right) corresponding to the northern part of the A3 region. Each plot shows the data time series and the wavelet power spectrum. Below the SAWP over the 0.5-24-hour band for *H* (solid) and *VTEC* (dashed) variations. The thin dashed line is 95% confidence interval for d*H* and the dash pointed line is the 95% level for d*VTEC*. The vertical solid line indicates the time of the storm commencement.

Figura 5a. Variaciones de *VTEC* y *H* en la estación GPS (izquierda) y el respectivo observatorio geomagnético (derecha) correspondientes a la parte norte de la región A3. Cada grafico muestra la serie temporal de datos y espectro de potencia ondeleta correspondiente. Debajo se muestra el SAWP (el promedio por escalas de la potencia ondeleta) para la banda de 0.5 a 24 horas calculada para las variaciones de *H* (línea solida) y *VTEC* (línea de segmentos) respectivamente. La línea punteada fina representa el 95% del intervalo de confianza para d*H* y la línea de puntos y rayas corresponde al nivel de 95% para d*VTEC*. La línea vertical solida indica el instante de comienzo de la tormenta.

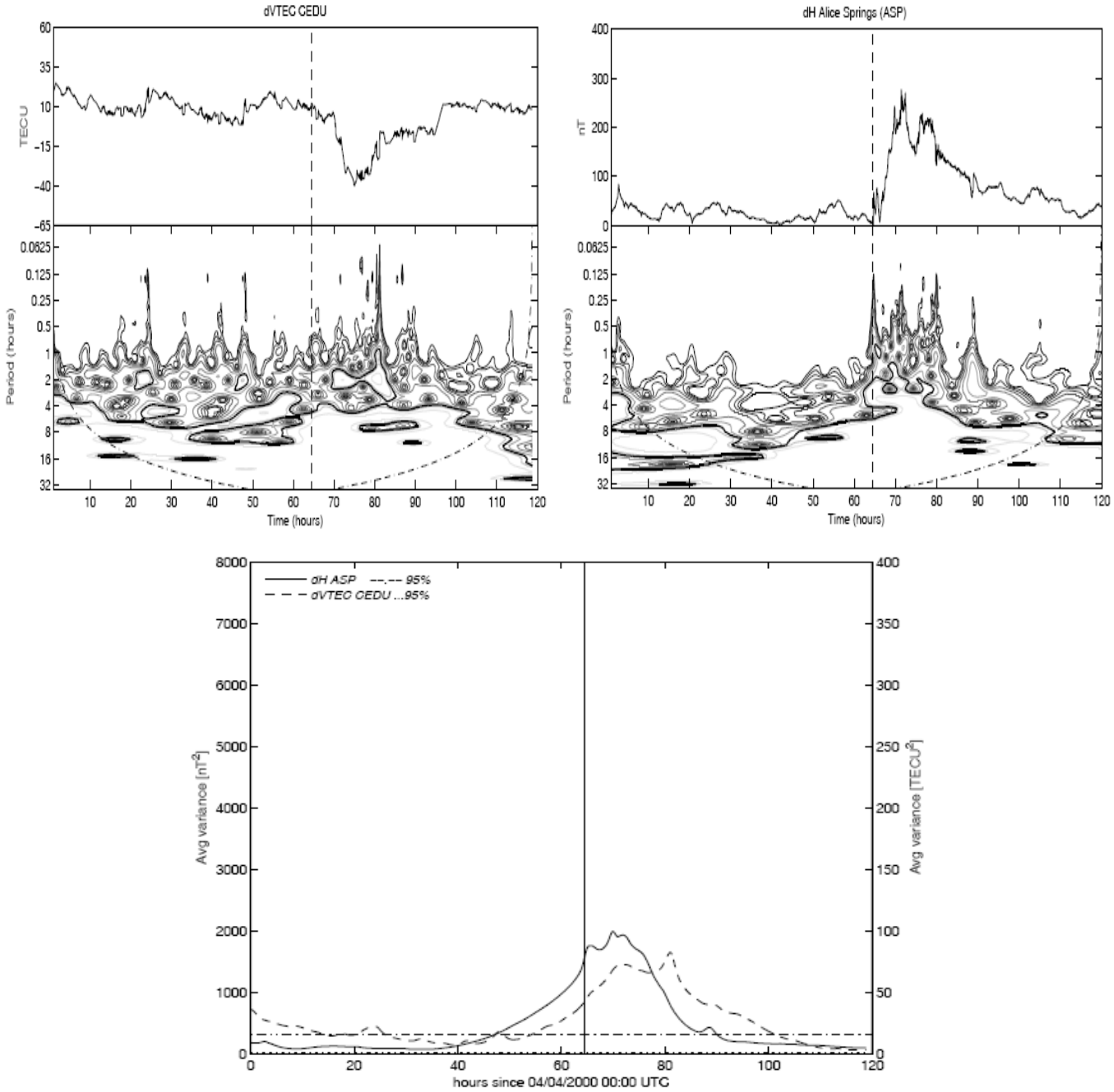

Figure 5b. The same as Fig. 5a for the southern hemisphere.
Figura 5b. Lo mismo que la Fig. 5a para el hemisferio austral.

The procedure explained above was applied to the April 2000 storm. Following, we will analyze the results of this wavelets application comparing them with the findings from other authors working on the same event.

The distinctive feature of Fig. 3a and 3b is the response of the ionospheric storm in both hemispheres at noon showing a positive and a negative phase. Effectively, the plots of SAWP for the 0.5-24 hour band show clear peaks reaching their maxima approximately at 69 hours (6 April, 21:00 UTC) for d*vTEC*. Likewise, the beginning of the positive phase of the ionospheric storm almost coincides with the beginning of the geomagnetic storm. This result agrees with Vijaya Lekshmi et al. (2011) who asseverated that the positive ionospheric storms occur frequently in

the morning-noon local time area of the geomagnetic main phase onset. The last is expected provided that the positive storms are linked to daytime photoionization mechanism. Both the Figure 3a and the Figure 3b show a clear maximum in d*H* in 72 hours (7 April, 00:00 UTC). This feature should also be associated with the simultaneous maximum in the solar wind pressure and the IMF indicating the closing of the magnetosphere. Besides the double peak structure of the maxima SAWP on d*H* variations coincide with the beginning of the geomagnetic storm recovery phase (Huttunen et al. 2002). Moreover another SAWP d*H* maximum can be observed in Figure 3a at approximately 2.5 hours (4 April-, 2:30 UTC). The last obey to an increase of the solar wind flow pressure and a sign change of Bz(IMF) (see Figure 1). In addition, the SAWP plot in figure 3a for the north hemisphere shows a maximum at the beginning of the positive phase of the ionospheric storm and another distinguishable feature in d*vTEC* near 87 hours (7 April, 15:00 UTC). This last should obey to an anomalous fluctuation during the recovery of the negative phase of the ionospheric storm in USNO GPS station.

Huang (2008) studied the ionospheric disturbances caused by the April 2000 storm event at middle and low latitudes. He presented ionospheric ion velocity and ion density values from DMSP (Defense Meteorological Satellite Program) satellites as well as TEC GPS at different sites from 30º to 40º magnetic latitudes. He observed a large increased of the ion density and an upward enhancement of ion velocity at middle latitudes only in the Northern hemisphere. That would explain the different amplitudes of the SAWP d*vTEC* at local noon (Area A1) showed at bottom in Figures 3a and 3b.

Moreover from our results, the highest power peak of geomagnetic variation is at A1 area but in the South. The reason for this is related to the location of the geomagnetic station LIV. It has geomagnetic latitude nearby to the 50º, so that it might be considered to be located at sub-auroral geomagnetic latitudes instead of at mid-ones.

When we studied the area A2, figures 4a and 4b show the effect of the terminator, which is a moving line that delimits the illuminated day side and the dark night side of the Earth. At sunrise the electron density begins to quickly augment due to photoionization. On the opposite, at sunset the electron density decays as the photoionization source disappears (Schunk and Nagy, 2000). Considering the effect of the terminator we have to be keep in mind that the civil twilight in the stations located in north hemisphere takes place at 21:12 LT and in the ones at the south hemisphere at 18:24 LT. Due to this there is not a positive phase of the ionospheric storm but there is a marked negative phase on both stations (VILL and SUTH) with a minimum near 85 hours (7 April, 13:00 UTC), and a beginning of decaying of the electrons concentration near the 75 hours (7 April, 3:00 UTC, that is, almost 10 hours later to the SSC of the storm), that is, just three hours after the start of the recovery phase of the geomagnetic storm. Consistently, the maxima of the SAWPs on *vTEC* residuals for both hemispheres appear near 80-83 hours (7 April, 08:00-11:00 UTC) though there are very broad peaks showing that the disturbances registered by the ionosphere at mid-latitudes during a geospheric storm at local dusk-evening are not so intense as in the area A1 but spread over a major period. Furthermore, both SAWP plots for the geomagnetic field in the A2 area show maxima at the beginning of the recovery phase, similar to the behavior showed by the geomagnetic field at A1 area.

The figures 5a and 5b showed us that when the ionospheric storm is observed in the morning sector, only a negative phase is perceived with a minimum near to 75 hours. Both plots of SAWP for d*VTEC* show a maximum near to 72-82 hours with similar extents in both hemispheres. Nevertheless, the GPS station CEDU shows a maximum in the wavelet power spectrum for the scales corresponding to periods between 0.5 and 4 hours causing then the double peak effect in the SAWP of d*VTEC* at GPS station CEDU. This feature can turn as a marked structure in the wavelet power spectrum that spreads up to 80 hours approximately. It might owe to an irregular variation of *vTEC* during the phase of recovery. Therefore we can think that this is just a locally anomalous feature not linked to the physical phenomenon of the storm. It is necessary to emphasize that in both hemispheres of A3 area the negative ionospheric storm begins nearer to the SSC of the geomagnetic storm than the negative phase at A2 area.

At one hand, Parks (1991) defined the recovery phase of the geomagnetic storm as the dissipation of the ring current and the posterior reaching of the normal undisturbed values. This process can take several days. On the other hand, Mendillo (2006) asseverated that the duration of the negative phase of the ionospheric storm is linked to the solar activity. In fact, the plasmaphere is depleted during a storm and the refilling time depends on the state of the F-layer previous to the event which is linked to the solar activity. He affirmed the negative phase of the ionospheric storm stays more than four days at solar maximum and up to two days at solar minimum.

Moreover, according to Liu et al. (2010), the time duration of the negative ionospheric storm in equinox are 9-10 and 9-15 hours depending on the local time. Belehaki and Tsagouri (2001) studied nighttime ionospheric storms at mid-latitudes. They showed that geomagnetic storms with initial phases followed by very fast evolving main phases produces a negative phase as a global effect; while in a gradual driven geomagnetic storm, a nighttime positive phase are frequently observed at mid and low latitudes.

The recovery phase of the geomagnetic field *H* after a storm takes 2 to 3 days depending on the solar conditions. Effectively, the former discussion is valid excluding a new arriving of a quick flux of solar wind to the magnetosphere.

In general from Figures 3 to 5, and analyzing just the ionospheric storm, we can affirm that the more noticeable the variation in the quantity of electrons with regard to the calm day is, narrower and clearer the SAWP peak will appear. Although the technique is not able to discriminate between positive and negative phase of the storm, it gives a way to quantify the maximum ionospheric variability relative to the ring current intensification.

In addition, when we apply the SAWP computation to analyze the effect of the geospheric event in the geomagnetic field, we notice that the maxima of the scale-averaged wavelet (solid lines in each figure 3 to 5) always happen nearby to the beginning of the respective recovery phase.

As a general rule, the maximum SAWP of the geomagnetic parameter falls quicker than the respective ionospheric SAWP maximum in both hemispheres. This could be linked to the different physical processes involved in the recovery phase of the ionospheric and geomagnetic storm.

Following Rishbeth (1963, in Mendillo 2006 pg. 18), even if the physical mechanisms accounting for geomagnetic and ionospheric perturbations during a storm event are not the same, there is rather a correlation of processes. Relative to the previous idea, we can mention Liu et al. (2010) as a reference focused in establishing the time delay between the geomagnetic activity during a storm and the ionospheric response.

Finally we also compute the normalized cross-correlation sequence of the two SAWP time series. The values of the time delay between the two moments for which the both (d*vTEC* and d*H*) SAWP time series indicate a maximum of cross-correlation. The time delay of the respective maximum of SAWP resulted about 0.5-1.5 hours for A1 area (noon), 12-15 hours for A2 area (dusk/evening) and 7-8 hours for the A3 sector (morning). All the recorded maxima of cross correlation are larger than 0.7.

Huang (2008) showed that plasma bubbles occurred within 1-3 h from the SSC and this is related to an eastward polarization electric field. Besides he proposed that the PPEF moved the mid-latitude F region to higher altitudes of low recombination causing thus an increase of plasma density that can be observed as a TEC increase. Such increase is not only observed by Huang (2008) over the entire latitudinal range of TEC GPS data but it also supports the existence of a PPEF provided that only electric fields can occur simultaneously at all latitudes.

Thus, the PPEF drove a positive storm phase at middle latitudes ionosphere on the dayside and such atmospheric disturbances related to the storm time electric field occurred within the first 1-2 h from the SSC (Huang, 2008), in agreement with our results for A1 area where the positive ionospheric storm at noon area is almost simultaneous to the geomagnetic variation.

In agreement with Prölss (2003), in the night sector polar heating zones caused by the storm induce winds superposed onto the equatorward normal diurnal wind circulation and carries the composition perturbation to mid-latitudes. The neutral composition disturbance causes the enhanced loss rate of ionospheric plasma producing thus a negative storm phase and this is the case for area A3 (morning) and A2 (dusk/evening). Our estimation of time delay values for the areas A2 and A3 are in agreement with those presented by the statistical study of Liu et al. (2010) for the mean time delay values for the negative storm considering both in equinox and at middle latitudes. In fact, the authors estimated 9 to 15 h for negative phase storms $Ap \geq 40$ in equinox depending on local time.

DISCUSSION AND SUMMARY

The average wavelet power spectrum was applied to GPS *vTEC* and *H* changes in order to quantify the variability of the ionospheric and geomagnetic perturbations triggered by a geospheric storm. Besides, the time delay between both maximal variations was also estimated using a normalized cross correlation. We chose the extensively studied event of April 2000 to test this wavelets application.

Both parameters, *vTEC* and *H* variations describing the ionospheric and geomagnetic storm behaviour, exhibit fairly clear structures. Moreover the respective wavelets power spectrums reveal that such structures contain information about variations from several minutes till hours.

At local noon (area A1) and irrespective of the hemisphere, we can observe a positive ionospheric storm that is followed by a negative storm. Both parameters (d*H* and d*vTEC*) reach the maximum values of power less than 1.5 hours to the culmination of the principal phase of the storm. The beginning of positive ionospheric storm is simultaneous with the beginning of geomagnetic storm. The effect of simultaneity is in good agreement with the findings of Huang et al. (2005), Huang (2008) and Meza et al. (2005).

On the other hand, when the geospheric storm is observed during the dusk/evening and the morning sectors (areas A2 and A3) only a negative ionospheric storm is observed and the parameter d*H* reaches the maximum values near the culmination of the principal phase of the storm whereas d*vTEC* maxima appear later. Analyzing the

negative ionospheric storm when it is in the morning sector, the d*vTEC* and d*H* show their maximum in SAWP closer each other than in the case of a negative ionospheric storm observed at the dusk/evening sector. On the other hand, similar behaviour is expected for all d*H* variations provided that all the selected stations are at magnetic mid-latitudes.

Not only the quicker ionospheric response is in the A1 sector where the onset of the SSC occurs at local noon, but also the most powerful ionospheric response occurred as expected. Besides the highest power peak of geomagnetic variation is at A1 area but in the South. The reason for this is related to the location of the geomagnetic station LIV. It has geomagnetic latitude nearby to the 50º, so that it might be considered to be located at sub-auroral geomagnetic latitudes instead of at mid-ones. In the dusk-evening and the morning sectors the ionospheric reactions are similar in the same area for both hemispheres.

The time delay of the respective maximum of SAWP resulted about 0.5-1.5 hours for A1 area (noon), 12-15 hours for A2 area (dusk/evening) and 7-8 hours for the morning sector. All the recorded maxima of cross correlation are larger than 0.7. These time delay values are in agreement with those presented by Liu et al. (2010) for the mean time delay values for the negative storm and the quick response of the positive storm considering both in equinox and at middle latitudes.

Huang (2008) clearly showed the existence of PPEF effects linked to the April 2000 storm event. He also showed that the PPEF drove a positive storm phase at middle latitudes ionosphere on the dayside and such atmospheric disturbances related to the storm time electric field occurred within the first 1-2 h from the SSC. This finding is in agreement with our results for A1 area where the positive ionospheric storm at noon area is almost simultaneous to the geomagnetic variation. The same author also observed a large increased of the ion density and an upward enhancement of ion velocity at middle latitudes only in the Northern hemisphere. That would explain the different amplitudes of the SAWP d*vTEC* at local noon (Area A1) showed at bottom in Figures 3a and 3b.

Following Prölss (2003), in the night sector polar heating zones caused by the storm induce winds superposed onto the equatorward normal diurnal wind circulation and carries the composition perturbation to mid-latitudes. This mechanism justifies the negative storm phase and this is the case for area A3 (morning) and the area A2 (dusk/evening).

Our estimation of time delay values for the areas A2 and A3 are in agreement with those presented by the statistical study of Liu et al. (2010) for the mean time delay values for the negative storm considering both in equinox and at middle latitudes. In fact, the authors estimated 9 to 15 h for negative phase storms $Ap \geq 40$ in equinox depending on local time.

The wavelet technique allows us to differentiate some features of geospheric storm behaviour from the *vTEC* variability and the geomagnetic field differences. We found out a reasonable agreement between these results and previous findings from other authors studying the same geospheric event or analyzing the local time dependency of the ionospheric responses to the geomagnetic storm variations. This support the usefulness of this assessment as a tool to analyze the storm ionospheric behaviors triggered by the geomagnetic storm perturbation.

In the near future we will work on more storms at different epoch of the year and different solar activity conditions. Thus, we will infer a statistics about the standards of behaviour when applying SAWP on variability of ionospheric and geomagnetic data.

Acknowledgements: This research is supported by ANPCyT grant PICT 2007-00405 and UNLP grant G095. The authors are grateful to World Data Centers for the free availability of the data: WDC-C, Kyoto University, Japan; Geomagnetic Information Node (GIN, British Geological Survey), Edinburgh, Scotland; N. Ness at Bartol Research Institute; CDAWeb (NASA, USA); and Scripps Institution of Oceanography from the University of California, San Diego (ftp://lox.ucsd.edu) and the Fédération des Services d´Analyse de Données Astronomiques et Geophysiques (Saint Maur des Fossés Cedex- France). Wavelet software was provided by C. Torrence and G. Compo, and modified for this application. The original file is available at URL: http://atoc.colorado.edu/research/wavelets/. The authors thank to two anonymous reviewers for helpful comments.

REFERENCES

Abreu A.J. de; Sahai Y., Fagundes P.R.; Becker-Guedes F., de Jesus R., Guarnieri F.L., Pillat V.G. Response of the ionospheric F-region in the Brazilian sector during the super magnetic storm in April 2000 observed by GPS. Adv. in Space Res. 45, 1322-1329, 2010.

Afraimovich, E.L., Ashkaliev, Ya.F., Aushev, V.M., Beletsky, A.B.,Vodyannikov, V.V., Leonovich, L.A., Lesyuta, O.S., Lipko, Yu.V., Mikhalev, A.V., Yakovets A.F. Simultaneous radio and optical observations of the mid-latitude

atmospheric response to a major geomagnetic storm of 6–8 April 2000. Journal of Atmospheric and Solar-Terrestrial Physics 64, 1943– 1955, 2002.
Andonov B., Mukhtarov P., Pancheva D. Empirical model of the TEC response to the geomagnetic activity over the North American region. Adv. in Space Res. 48, 1041–1048, 2011
Balan, N., K. Shiokawa, Y. Otsuka, T. Kikuchi, D. Vijaya Lekshmi, S. Kawamura, M. Yamamoto, and G. J. Bailey. A physical mechanism of positive ionospheric storms at low and mid latitudes through observations and modeling, J. Geophys. Res., 115, A02304, doi:10.1029/2009JA014515; 2010.
Belehaki A., Tsagouri I. Study of the Termospheric-Ionospheric Response to Intense Geomagnetic Storms at Middle Latitudes. Phys. Chem. Earth C., Vol. 26 Nº5, Pp. 353-357, 2001.
Boudouridis, A., Zesta, E.: Comparison of Fourier and wavelet techniques in the determination of geomagnetic field line resonances, J. Geophys. Res., 112, A08205, doi:10.1029/2006JA011922. 2007.
Daubechies, I.:Ten Lectures on Wavelets, CBMS-NSF Lecture Notes nr. 61, SIAM, 1992.
Foster, J.C.: Storm-time plasma transport at middle and high latitudes, J. Geophys. Res. 98, 1675–1689, 1993.
Foster, J. C., and Rich F. J.: Prompt midlatitude electric field effects during severe geomagnetic storms, J. Geophys. Res., 103(A11), 26,367–26,372, doi:10.1029/97JA03057, 1998.
Fuller-Rowell; T.J, Codrescu, M.V., Moffett, R.J. and Quegan, S.: Response of the thermosphere and ionosphere to geomagnetic storms. J. Geophys. Res. 99, 3893–3914, 1994.
Ge, Z.: Significance tests for the wavelet power and the wavelet power Spectrum. Ann. Geophys., 25, 2259–2269, 2007.
Gomez, L., Sabbione, J.I., Van Zele, M.A., Meza, A., Brunini, C.: Determination of a geomagnetic storm and substorm effects on the ionospheric variability from GPS observations at high latitudes, Journal of Atmospheric and Solar-Terrestrial Physics, 69, 955–968, 2007.
Holschneider, M.: Introduction to Continuous Wavelet Analysis in Wavelets in the Geosciences, 1-71. Lecture Notes in Earth Sciences, 90. Klees and Haagmans eds. Springer-Verlag, Berlin. Germany.2000.
Huang, C. S., Foster, J. C., Goncharenko, L. P., Erickson, P. J., Rideout, W. and A. J. Coster: A strong positive phase of ionospheric storms observed by the Millstone Hill incoherent scatter radar and global GPS network, *J. Geophys. Res., 110* , A06303, doi:10.1029/2004JA010865, 2005.
Huang, C. S., Global characteristics of ionospheric electric fields and disturbances during the first hours of magnetic storms. Adv. Space Res. 41, 527-538, 2008.
Huttunen, K. E. J., Koskinen, H. E. J., Pulkkinen, T. I., Pulkkinen, A., Palmroth, M., Reeves, E. G. D. and Singer, H. J.: April 2000 magnetic storm: Solar wind driver and magnetospheric response, J. Geophys. Res., 107(A12), 1440, doi:10.1029/2001JA009154, 2002.
Iyemori, T., Araki, T., Kamei, T., Takeda, M.: Mid-latitude Geomagnetic Indices “ASY” and “SYM” for 1999 (Provisional). http://wdc.kugi.kyoto-u.ac.jp/aeasy/asy.pdf.
Iyemori, T**.**, Formation of storm-time ring current and the Dst field: Some recent topics, in Magnetospheric current systems, ed. by S.Ohtani et al., AGU Monograph, 118, 331-338, 2000.
Jakowski, N., Putz, E., and Spalla, P.0.: Ionospheric storm characteristics deduced from satellite radio beacon observations at three European stations, Ann. Geophys., 8, 343–352, 1990.
Kumar, P., Foufoula-Georgiou, E.: Wavelet Analysis in Geophysics: An Introduction in Wavelets in Geophysiscs, 1-43, Kumar and Foufoula-Georgiou eds., Academic Press. San Diego. U.S.A. 1994.
Kumar, P., Foufoula-Georgiou, E.: Wavelet Analysis for Geophysical Applications. Reviews of Geophysics, 35, 4, 385–412, 1997.
Kumar S., Sharma S., Chandra H. Interplanetary origin of magnetic storms and their F2-region responses at the equatorial anomaly Adv. In Space Res. 37, 1777-1783, 2006.
Lastovicka, J.: Monitoring and forecasting of ionospheric space-weather: effects of geomagnetic storms, Journal of Atmospheric and Solar-Terrestrial Physics, 64, 697-705, 2002.
Lee, C.-C., J.-Y. Liu, M.-Q. Chen, S.-Y. Su, H.-C. Yeh, and K. Nozaki (2004), Observation and model comparisons of the traveling atmospheric disturbances over the Western Pacific region during the 6–7 April 2000 magnetic storm, J. Geophys. Res., 109,A09309, doi:10.1029/2003JA010267, 2004.
Liu L., Wan W., Lee C.C., Ning B., Liu J.Y. The low latitude ionospheric effects of the April 2000 magnetic storm near the longitude 120º E. Earth Planets Space, 56, 607-612, 2004.
Liu J., Zhao B., Liu L. : Time delay and duration of ionospheric total electron content responses to geomagnetic disturbances. Ann. Geophys., 28, 795-805, 2010.
Lu, G., Richmond, A. D., Roble, R. G. and Emery B. A.: Coexistence of ionospheric positive and negative storm phases under northern winter conditions: A case study, J. Geophys. Res., 106, 24,493–24,504, doi:10.1029/2001JA000003, 2001.

Mendes, O.Jr., Oliveira Domingues, M., Mendes da Costa, A., Clúa de Gonzalez, A.L.: Wavelet analysis applied to magnetograms: Singularity detections related to geomagnetic storms, Journal of Atmospheric and Solar-Terrestrial Physics, 67, 1827–1836, 2005.
Mendillo, M.: Storms in the ionosphere: patterns and processes for total electron content, Rev. Geophys. 44, RG 4001 doi: 10.1029/2005RG000193, 2006.
Menvielle, M., Berthelier, A.: The K-derived planetary indices: Description and availability, Rev. Geophys., 29(3), 415–432, doi:10.1029/91RG00994, 1991.]
Meza, A., Van Zele, M. A., Brunini, C., Cabassi, I. R.: Vertical electron content and geomagnetic perturbations at mid- and sub-auroral southern latitudes during geomagnetic storms, Journal of Atmospheric and Solar-Terrestrial Physics, 67, 315-323, 2005.
Parks G.K. Physics of the Space Plasma, An Introduction. Addison- Wesley Publishing Company, 1991.
Prölss, G.W.: On explaining the local time variation of ionospheric storm effects, Ann. Geophys., 11, 1-9, 1993.
Prölss, G.W.: Ionospheric F-region storms in Handbook of Atmospheric Electrodynamics Vol. 2 (H. Volland ed.), 195, CRC Press, Boca Raton, 1995.
Prölss, G.W.: Physics of the Earth's Space Environment: An Introduction. Springer-Verlag, Berlin, 2004.
Schunk R.W and Nagy A.F.: Ionospheres: Physics, Plasma Physics and Chemistry. Cambridge University Press. 2000
Swisdak, M., Huba, J. D., Joyce, G. and Huang, C.-S.: Simulation study of a positive ionospheric storm phase observed at Millstone Hill, *Geophys. Res. Lett.*, 33, L02104, doi:10.1029/2005GL024973, 2006.
Torrence, C., Compo, G.P.: A Practical Guide to Wavelet Analysis. Bulletin of the American Meteorological Society, 79, 1, 61-78, 1998.
Tsagouri, I. and Belehaki A.: A new empirical model of middle latitude ionospheric response for space weather applications, Advances in Space Research, 37 (2): 420-425 Sp. Iss., 2006
Tsurutani B.T.; Zhou X.-Y., Arballo J.K., Gonzalez W.D., Lakhina G.S., Vasyliunas V., Pickett J.S., Araki T. , Yang H., Rostoker G., Hughes T.J., Lepping R.P., Berdichevsky D. Auroral zone dayside precipitation during magnetic storm initial phases. J. of Atmosph. and Solar-Terrestrial Phys. 63, 513–522. 2001.
Vijaya Lekshmi, D., N. Balan, S. Tulasi Ram, and J. Y. Liu, Statistics of geomagnetic storms and ionospheric storms at low and mid latitudes in two solar cycles, J. Geophys. Res., 116, A11328, doi:10.1029/2011JA017042, 2011
Werner, S., Bauske, R., Prölss G.W.: on the origin of positive ionospheric storms. Adv. Space Res., 24, Nr 11, 1485-1489, 1999.

Recibido: 13-9-2012
Aceptado: 4-2-2013